Journal of Power Sources 196 (2011) 8701–8705

Contents lists available at ScienceDirect

Journal of Power Sources

journal homepage: www.elsevier.com/locate/jpowsour

Short communication

SnO_2 nanocrystals deposited on multiwalled carbon nanotubes with superior stability as anode material for Li-ion batteries

Jianguo Ren, Junbing Yang*, Ali Abouimrane, Dapeng Wang, Khalil Amine*

Chemical Sciences and Engineering Division, Argonne National Laboratory, 9700 South Cass Avenue, Argonne, IL 60439, USA

ARTICLE INFO

Article history:
Received 4 May 2011
Received in revised form 7 June 2011
Accepted 7 June 2011
Available online 21 June 2011

Keywords:
Li ion batteries
Tin dioxide
Carbon nanotube
Anode
Ethylene glycol

ABSTRACT

We report a novel ethylene glycol-mediated solvothermal-polyol route for synthesis of SnO_2–CNT nanocomposites, which consist of highly dispersed 3–5 nm SnO_2 nanocrystals on the surface of multiwalled carbon nanotubes (CNTs). As anode materials for Li-ion batteries, the nanocomposites showed high rate capability and superior cycling stability with specific capacity of 500 mAh g^{-1} for up to 300 cycles. The CNTs served as electron conductors and volume buffers in the nanocomposites. This strategy could be extended to synthesize other metal oxides composites with other carbon materials.

The lithium-ion battery (LIB) has been widely regarded as the most promising power source for the plug-in hybrid electric vehicle (PHEV) and electric vehicle (EV). New-generation electrode materials with high energy, high rate capability, and good safety performance have been extensively studied to meet the challenging requirements for PHEV and EV applications [1]. At the moment, the state-of-the-art anode material for the LIB is graphite, which has a theoretical capacity of 372 mAh g^{-1} [2]. However, tin-based oxides have been considered as a potential substitute for graphite because of their higher theoretical reversible capacity (e.g., 781 mAh g^{-1} for SnO_2) [3]. The practical application of SnO_2, so far, is hampered by poor cyclability arising from the large volume change after repetitive charging and discharging, which causes mechanical failure and the loss of electrical contact [4]. To overcome this problem, many researchers are focusing on synthesis of SnO_2 nanoparticles, which are able to better accommodate the mechanical stress experienced during volume changes [5]. Another approach is the use of carbon as matrix support on which SnO_2 nanoparticles are attached [6]. Among various kinds of carbon materials, the carbon nanotube is attractive due to its high electrical conductivity, high aspect ratio, remarkable thermal conductivity, and good mechanical properties, which can improve the electrode's reversible capacity and rate capability [7].

Recently, the polyol method has been found to be well-suited for the preparation of nanoscale metal oxides [8]. The basis of this method is a forced hydrolysis reaction when heating proper precursors in a viscous and high-boiling-point polyol [9]. For example, ethylene glycol (EG, $HO–CH_2CH_2–OH$) possesses a high boiling point of 197.3 °C. The polyols can act as a stabilizer, limiting particle growth and prohibiting agglomeration. Due to the high temperature that can be applied during the process of synthesis, highly crystalline oxides are frequently obtained without any subsequent heat treatment [10].

Herein, we report a simple solvothermal-polyol route for the synthesis of SnO_2–CNT nanocomposites, which consist of highly dispersed SnO_2 nanocrystals with diameters of 3–5 nm that are deposited on the outer surface of CNTs. Their electrochemical activity is characterized in comparison with pure SnO_2 powders.

1. Experimental

All of the reactants were of analytical grade and used without further purification. Multiwalled carbon nanotubes (MWCNTs) with an outer diameter of 50–100 nm and length of 5–10 μm were purchased from Nanostructured & Amorphous Materials Inc. and purified by refluxing in concentrated H_2SO_4/HNO_3 (1:1 by volume) at 120 °C for 2 h, followed by washing with high purity water and filtration. This process will result in the formation of functional groups such as acidic groups that can help retain the SnO_2 during the deposition process.

We fabricated SnO_2–CNT nanocomposites via a solvothermal method using ethylene glycol (EG, from Sigma–Aldrich, USA) as solvent in a 23-mL Teflon-lined autoclave. Typically, 300 mg $SnCl_4{\cdot}5H_2O$ (Sigma–Aldrich, USA) was dissolved in 15 mL of EG.

* Corresponding authors.
E-mail addresses: yangj@anl.gov (J. Yang), amine@anl.gov (K. Amine).

0378-7753/$ – see front matter © 2011 Elsevier B.V. All rights reserved.
doi:10.1016/j.jpowsour.2011.06.036

Subsequently, 100 mg CNTs was added, and the suspension was sonicated for 1 h by a probe sonicator (Branson Digital Sonifier). The suspension was transferred into a Teflon-lined stainless steel autoclave and kept at 210 °C for 12 h. The precipitate was separated by centrifugation and washed with acetone three times before drying at 120 °C for 2 h to obtain the final SnO_2–CNT nanocomposites. Pure SnO_2 powders were prepared in a similar process except for the absence of CNTs for comparison purpose.

The crystal structure of the obtained samples was characterized by X-ray diffraction (XRD) using a Siemens D5000 diffractometer with Cu-Kα radiation (λ = 1.5406 Å). The morphology of the samples was investigated by scanning electron microscopy (SEM) using a Hitachi S-4700-II microscope. A transmission electron microscope (TEM, JEOL 2100) was used to analyze the SnO_2 nanocrystals on the surface of CNTs. Thermogravimetric analysis (TGA, NETZSCH STA 449 *F3*) was performed to determine the content of SnO_2 in the composite using a heating rate of 5 °C min^{-1} in an air atmosphere from room temperature to 1000 °C. X-ray photoelectron spectroscopy (XPS, Kratos AXIS-165 surface analysis system with a monochromatic Al K X-ray source) was used to determine the chemical composition near the surface of CNTs.

Electrochemical characterization was carried out by galvanostatic cycling of CR2032 coin cells using lithium foil as the anode. The working electrode was made of 70 wt% active SnO_2–CNT composite materials (or pure SnO_2 powders), 20 wt% acetylene black, and 10 wt% poly(vinylidene fluoride) binder. The electrolyte was 1.2 M $LiPF_6$ dissolved in a mixture of ethylene carbonate and ethyl methyl carbonate (3:7 by weight). The cells were assembled in an argon-filled glove box and were tested in the voltage range of 5 mV–2 V at room temperature. Cyclic voltammetry was also carried out in a Solartron 1470 E instrument in the voltage range of 5 mV–3 V at a scanning rate of 0.2 mV s^{-1}. The AC impedance spectra were measured in the frequency range of 10^{-2} to 10^6 Hz after the cells had been discharged and charged for five cycles.

2. Results and discussion

The solvothermal-polyol process combined with forced hydrolysis can effectively convert $SnCl_4$ to crystalline SnO_2 without further heat treatment. In this process, polyol serves as a chelating agent [11,12]. The formation of SnO_2 nanocrystals by this process can be attributed to the following reactions:

$$SnCl_4 + C_2H_6O_2 = Sn(C_2H_6O_2)Cl_4 \quad (1)$$

$$Sn(C_2H_6O_2)Cl_4 + 4OH^- + 4H^+ = Sn(C_2H_6O_2)(OH)_4 + 4HCl \quad (2)$$

$$Sn(C_2H_6O_2)(OH)_4 = SnO_2 + 2H_2O + C_2H_6O_2 \quad (3)$$

First, EG chelated $SnCl_4$ complexes are formed (reaction (1)). Then, the forced hydrolysis of the complexes follows with a small amount of water from $SnCl_4{\cdot}5H_2O$ (reaction (2)). It is expected that high concentrations of H^+ and OH^- ions are generated through water dissociation near the critical point under the solvothermal condition in the sealed Teflon reactor. Finally, the hydroxide is converted to SnO_2 by dehydration (reaction (3)). Fig. 1a shows a SEM image of the bare MWCNTs, which exhibit a smooth outer surface with diameters around 50–100 nm and several micrometers in length. For comparison, Fig. 1b shows an SEM image of the SnO_2–CNT nanocomposite, in which SnO_2 is considered to be selectively nucleated and uniformly deposited on the surface of CNTs by the solvothermal-polyol process. No obvious separated SnO_2 bulk particles are evident apart from those deposited on CNTs. The CNTs coated with SnO_2 are entangled and interconnected to form a uniform network with a three-dimensional structure. For further investigation of the morphology and distribution of SnO_2 nanocrystals on the surface of CNTs, Fig. 2 shows a TEM image of a SnO_2–CNT nanocomposite. The observed SnO_2 nanoparticles are highly crystalline with particle size of 3–5 nm in diameter and are closely attached onto the surface of the CNTs. The aligned lattice fringes of the nanoparticles and CNTs are apparent, with adjacent lattice spacing of about 0.32 nm, corresponding to the (1 1 0) plane of SnO_2, and a carbon layer separation of 0.34 nm assigned to the (0 0 2) plane of CNTs [4].

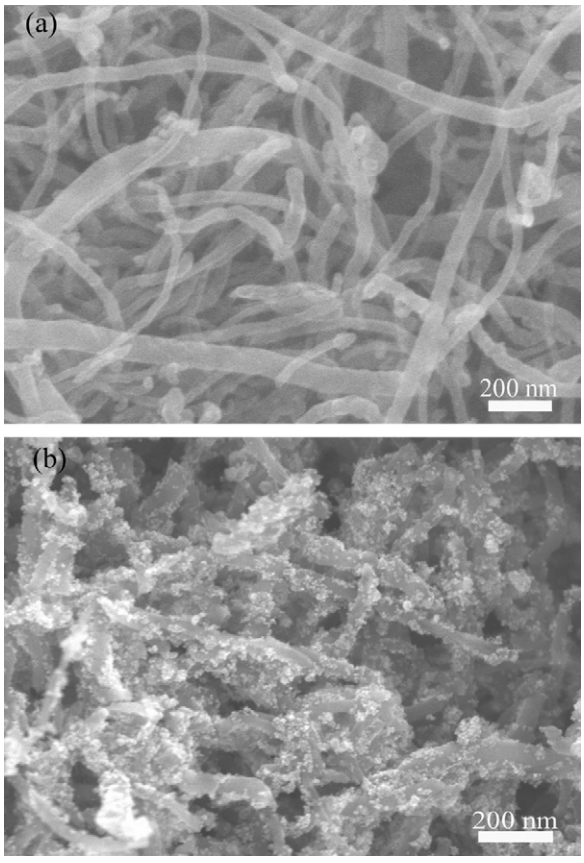

Fig. 1. (a) SEM image of bare MWCNTs and (b) SEM image of SnO_2–CNT nanocomposite.

We performed TGA from room temperature to 1000 °C in air at 5 °C min^{-1} to estimate the SnO_2 loading amount in the nanocomposite, since CNTs can be burned away in air around 360 °C. As shown in Fig. 3, most of the weight loss of SnO_2–CNT nanocomposite had occurred by about 700 °C, and the amount of weight

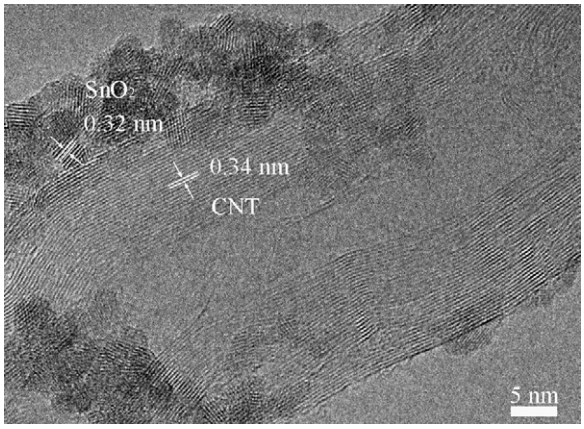

Fig. 2. High-resolution TEM image of SnO_2–CNT nanocomposite with lattice spacing.

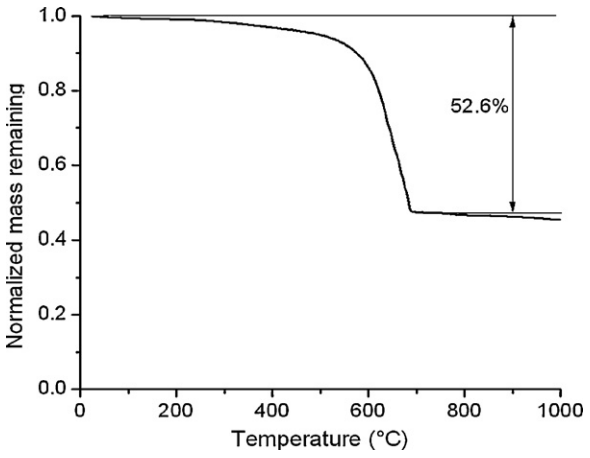

Fig. 3. TGA curve of SnO_2–CNT nanocomposite heated in air.

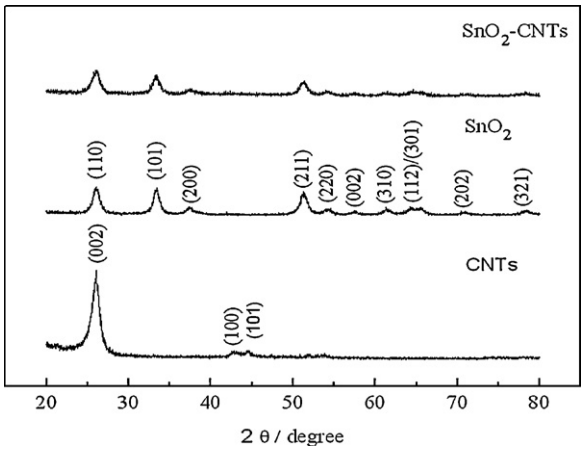

Fig. 4. XRD patterns of the CNTs, pure SnO_2 powders, and SnO_2–CNT nanocomposites.

loss was measured to be 52.6%, meaning that the weight percentage of SnO_2 in the nanocomposite is 47.4%. Fig. 4 shows the XRD patterns of CNTs, SnO_2 powders, and SnO_2–CNT nanocomposites. The CNTs present a main characteristic peak at about $2\theta = 26^\circ$, corresponding to the (0 0 2) reflection. All intense peaks in the bare SnO_2 powders can be well indexed to rutile SnO_2 (JCPDS Card No. 41-1445, space group *P42/mnm*, $a = b = 4.738$ Å, $c = 3.187$ Å). For the SnO_2–CNT nanocomposite, all peaks correspond to the reflections

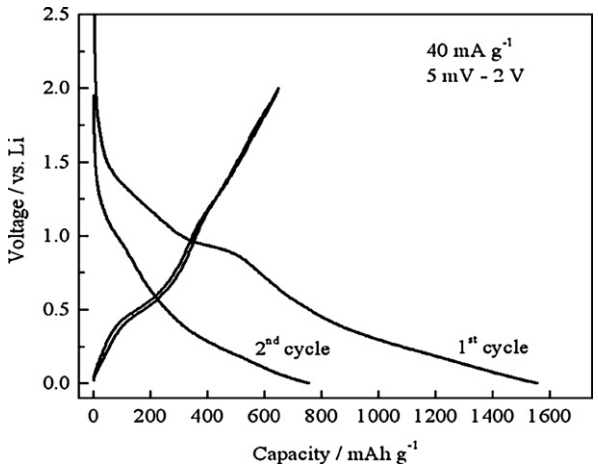

Fig. 6. First and second discharge/charge voltage profiles of SnO_2–CNT nanocomposite electrode at a rate of 40 mA g^{-1}.

of SnO_2, among which the (1 1 0) reflection of SnO_2 overlaps with the (0 0 2) reflection of CNTs.

The above results suggest that the SnO_2 nanocrystals were nucleated heterogeneously and grown on the external surface of CNTs by the solvothermal-polyol process. We believe that the formation mechanism might be the adsorption of tin cations on the functional groups of the acid-treated CNT surface by electrostatic attraction. Fig. 5 presents the XPS O1s peaks of the pristine CNTs and that obtained after the H_2SO_4/HNO_3 treatment. Deconvolution of the XPS O1s peak confirmed the presence of carbonyl and carboxyl onto the CNT surfaces at 532.2 and 533.5 eV, respectively. Study of the acid-treated CNTs showed an increase of the carboxylic amount in the O1s regions as compared to the pristine CNTs (Fig. 5d). We believe that such oxygen-containing functional groups will introduce some negatively charged sites on the carbon surface, which can absorb the tin cations and promote in situ heterogeneous nucleation and growth of SnO_2 nanocrystals.

Fig. 6 shows the charge/discharge voltage profiles of half cell SnO_2–CNT/Li during the first and second cycles. In the first discharge, a typical plateau around 0.8 V, corresponding to the formation of a solid-electrolyte interfacial (SEI) layer and the reaction of SnO_2 with lithium to form amorphous Li_2O and nanocrystalline Sn[14], is observed. This plateau disappeared in the second cycle, meaning the conversion reaction from SnO_2 to Sn is irreversible. To further understand the reaction mechanism, cyclic voltammetry profiles were obtained for the SnO_2–CNT electrode from the first to the fifth cycle, as shown in Fig. 7. A sharp reduction peak at

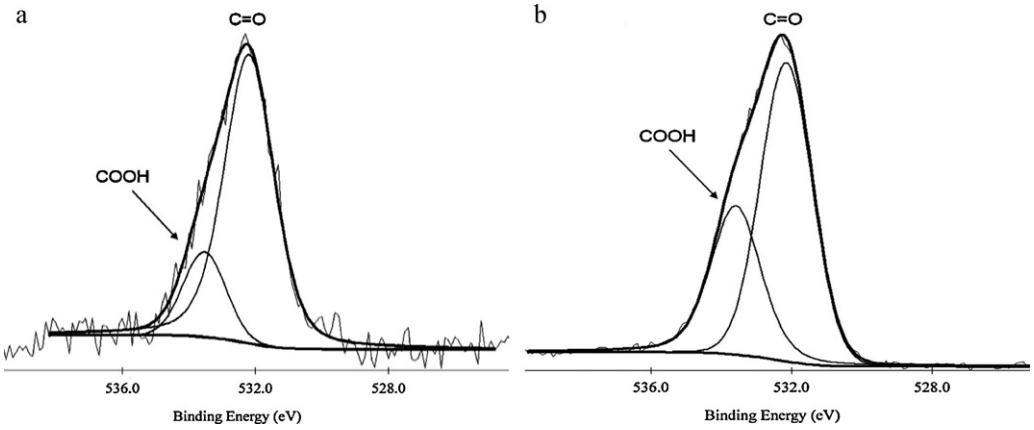

Fig. 5. XPS spectra of the O1s regions of (a) the pristine CNTs and (b) the oxidized CNTs.

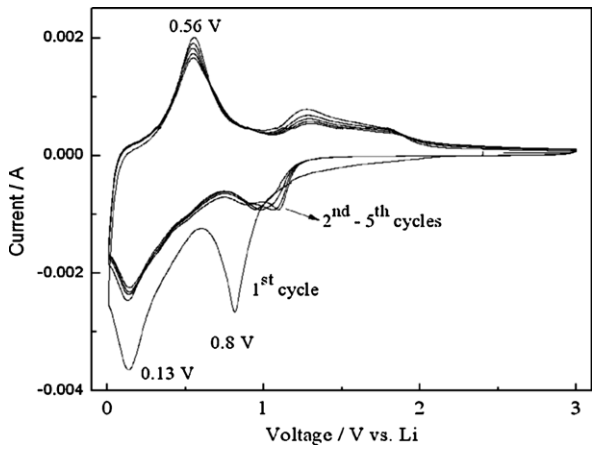

Fig. 7. Cyclic voltammetry profiles of SnO_2–CNT electrode from first to fifth cycle.

0.8 V was observed in the first cycle, which can be attributed to the formation of an SEI layer and the irreversible reduction reaction of SnO_2:

$$SnO_2 + 4Li^+ + 4e^- = Sn + 2Li_2O \quad (4)$$

The cathodic peak at 0.13 V and anodic peak at 0.56 V can be assigned to the reversible alloying/dealloying reaction of nanocrystalline Sn with lithium:

$$Sn + xLi^+ + xe^- = Li_xSn \quad (0 \le x \le 4.4) \quad (5)$$

The results of the rate performance for a pure SnO_2 electrode and a SnO_2–CNT nanocomposite electrode are shown in Fig. 8. In this case, the 1 C rate is 600 mA g^{-1}. The pure SnO_2 electrode exhibits a higher initial specific capacity than SnO_2–CNT nanocomposite electrode when cycled at low rates, less than 1 C. While at rates higher than 3 C, the SnO_2–CNT nanocomposite electrode shows larger capacity compared to the pure SnO_2. This result can be attributed to the CNTs, which serve as an effective electron conductor, that prevent SnO_2 nanocrystals from agglomeration. To better demonstrate the effect of CNTs on the electronic conductivity of the SnO_2–CNT nanocomposite, the AC impedance spectra were measured when the cells were discharged and charged for five cycles, as shown in Fig. 9. Both electrodes exhibited Nyquist plots consisting of a depressed semicircle at high frequency, which is correlated with the electron transfer resistance on the electrode interface [13]. The SnO_2–CNT nanocomposite provides a smaller diameter of the high-frequency semicircle compared with that of the SnO_2 electrode. This finding indicates that good electronic contact was maintained

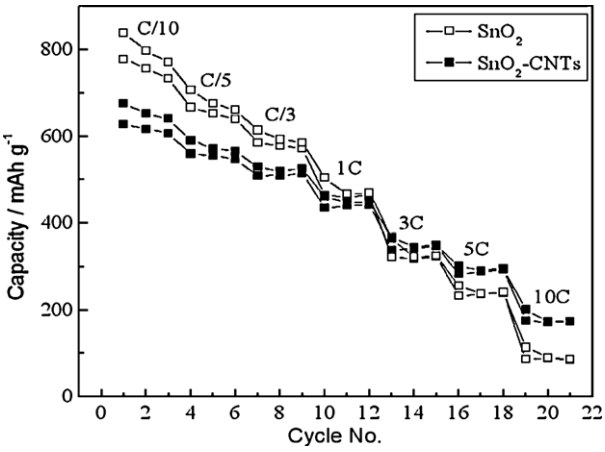

Fig. 8. Rate performance of pure SnO_2 and SnO_2–CNT nanocomposite electrodes.

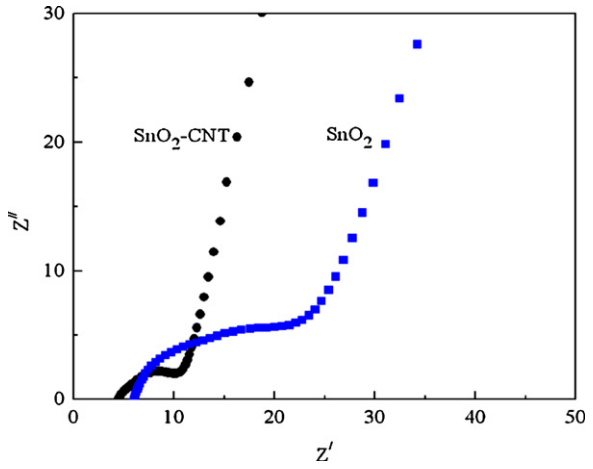

Fig. 9. AC impedance profiles of pure SnO_2 and SnO_2–CNT nanocomposite electrodes after five discharge/charge cycles.

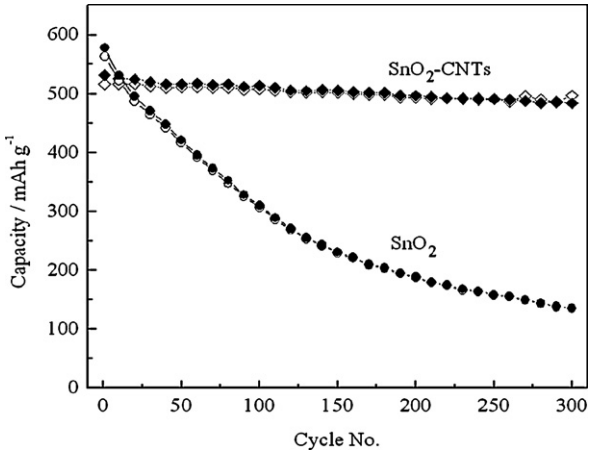

Fig. 10. Charge/discharge capacities of the pure SnO_2 and SnO_2–CNT nanocomposite electrodes at a rate of 200 mA g^{-1}.

after repeated lithium insertion and extraction as a result of the strong adherence and thus direct electronic connection of the SnO_2 nanocrystals on the surface of the CNTs.

Fig. 10 shows the cycling performance of both electrodes in the potential range of 5 mV–2 V at a current of 200 mA g^{-1}. As expected, the SnO_2–CNT nanocomposite electrode exhibited excellent capacity retention up to 300 cycles. The charge capacities of both electrodes after 300 cycles were 497 mAh g^{-1} and 135 mAh g^{-1}, respectively. We attribute the superior cycling stability of the SnO_2–CNT nanocomposite to its special hybrid structure.

Furthermore, the volumetric capacity density was discussed. In the case of SnO_2–CNT electrode, the thickness of the electrode was 15 μm (Cu current collector excluded), and the area of the disk was 1.6 cm^2 with the loading of active material (SnO_2–CNT) of 1.26 mg. The volumetric capacity density was 0.5 mAh mg^{-1} × 1.26 mg/(1.6 cm^2 × 0.0015 cm) = 262.5 mAh cm^{-3}.

3. Conclusion

In summary, a SnO_2–CNT nanocomposite was successfully synthesized by a simple solvothermal-polyol route using ethylene glycol as media. The highly dispersed SnO_2 nanocrystals with crystal size of 3–5 nm were uniformly deposited onto the surface of CNTs. As anode material for Li-ion battery, the nanocomposite presented a superior cycling stability up to 300 cycles with a capacity of 500 mAh g^{-1}. Such good stability was ascribed to the strong

adhesion of SnO_2 nanocrystals on the CNT support, which has high electronic conductivity and possesses good flexibility. The strategy presented in this paper could be extended to the synthesis of other metal oxide (e.g., MnO_x, FeO_x, CoO_x, TiO_2, and ZnO) composites with different carbon materials.

Acknowledgments

This research was funded by the U.S. Department of Energy, FreedomCAR and Vehicle Technologies Office. Argonne National Laboratory is operated for the U.S. Department of Energy by UChicago Argonne, LLC, under Contract DE-ACO2-06CH11357.

References

[1] K. Amine, I. Belharouak, Z.H. Chen, T. Tran, H. Yumoto, N. Ota, S.T. Myung, Y.K. Sun, Adv. Mater. 22 (2010) 3052–3057.
[2] F.M. Courtel, E.A. Baranova, Y.A. Lebdeh, I.J. Davidson, J. Power Sources 195 (2010) 2355–2361.
[3] G.D. Du, C. Zhong, P. Zhang, Z.P. Guo, Z.X. Chen, H.K. Liu, Electrochim. Acta 55 (2010) 2582–2586.
[4] L. Noerochim, J.Z. Wang, S.L. Chou, H.J. Li, H.K. Liu, Electrochim. Acta 56 (2010) 314–320.
[5] S.H. Ng, D.I. Santos, S.Y. Chew, D. Wexler, J. Wang, S.X. Dou, H.K. Liu, Electrochem. Commun. 9 (2007) 915–919.
[6] H.X. Zhang, C. Feng, Y.C. Zhai, K.L. Jiang, Q.Q. Li, S.S. Fan, Adv. Mater. 21 (2009) 2299–2304.
[7] Z. Wen, Q. Wang, Q. Zhang, J. Li, Adv. Funct. Mater. 17 (2007) 2772–2778.
[8] J.Y. Kim, K.H. Kim, S.H. Park, K.B. Kim, Electrochim. Acta 55 (2010) 8056–8061.
[9] X.C. Jiang, Y.L. Wang, T. Herricks, Y.N. Xia, J. Mater. Chem. 14 (2004) 695–703.
[10] H. Zhang, J.B. Wu, C.X. Zhai, N. Du, X.Y. Ma, D.R. Yang, Nanotechnology 18 (2007) 455604–455610.
[11] D. Caruntu, Y. Remond, N.H. Chou, M.J. Jun, G. Caruntu, J. He, G. Goloverda, C. Connor, V. Kolesnichenko, Inorg. Chem. 41 (2002) 6137–6146.
[12] R.J. Joseyphus, T. Matsumoto, H. Takahashi, D. Kodama, K. Tohji, B. Jeyadevan, J. Solid State Chem. 180 (2007) 3008–3018.
[13] P.F. Gao, Y.N. Nuli, Y.S. He, J.Z. Wang, A.I. Minett, J. Yang, J. Chen, Chem. Commun. 46 (2010) 9149–9151.